Article

Bull. Volcanol. Soc. Japan
Vol. 58 (2013) No. 1, pp. 291-306

Ellipse-approximated Isopach Maps for Estimating Ashfall Volume at Sakurajima Volcano

Yasuhisa TAJIMA*, Keiji TAMURA**, †, Takao YAMAKOSHI**,
Akira TSUNE*** and Shinjiro TSURUMOTO****, ††

(Received May 6, 2011; Accepted January 7, 2013)

In studies of volcanic tephra, it is usual that the overall volume of tephra is estimated ashfall volumes based on representative locations within the ashfall area. The precision of the volume estimation largely depends on the number of the locations. However, in the case of ongoing eruptions on island volcanoes, such as Sakurajima volcano, the observation locations are usually limited. We therefore have developed a practical method for estimating ashfall volume and distribution in such case. The method approximates the distribution of ashfall as ellipses, with the distribution area (A) and thickness or weight of deposit (T) determined by $A=\alpha T^{-1}$. The ellipse-approximated isopachs can be determined by using the direction of the ellipse axis and ashfall data at two points. In determing the ellipse axis exactly, we usually need additional ashfall amounts from the other locations. We set 37 samplers around Sakurajima volcano, and retrieved the samplers 15 times, from April to December, 2008. Using the propose method, we are able to determine the volume of ash produced by small, continuous eruptions.

Key words: ashfall distribution; isopach; ellipse approximation; volume estimation; Sakurajima volcano

1. Introduction

The difficulty of ashfall volume estimation for small islands or short intermittent eruptions in Japan is a major issue, when forecasting the progress of volcanic eruptions. Hence, we propose a tool for estimating ashfall volume using limited ashfall observation locations as inputs. Such tool is useful in the case of ongoing eruptions when observation locations are usually limited.

Many authors have proposed methods to calculate the distribution or volume of pyroclastic falls. The most advanced method is to produce an isopach map (lines of equal thickness) of tephra deposits, based on many points determined by geological surveys. Other approaches to volumetric calculations include simulation models based on the dynamics of the eruption column and existing models or codes (Ishimine, 2007). An isopach is a contour line that shows the same thickness of tephra for a given area. Whole ashfall volume can be estimated using isopach map by applying integral calculus. Many studies have shown that tephra thickness decreases exponentially with distance from the vent. Thorarinsson (1954) showed important results related to the exponential decrease in tephra thickness with increasing distance from the source. Porter (1973) considered that the correlation of thickness and distance followed a power relationship for Hawaiian tephra. Suzuki (1981) presented a logarithm approximation method that explained these correlations.

If the area and tephra thickness are correlated, then the volume of tephra can be deduced. Rose *et al*. (1973) estimated ashfall volume by integrating the plot of log (T) against log(A) with distribution area (A) and thickness or weight of deposit (T). Recently, ashfall deposits were shown to follow exponential decreases of log(T) against log ($\sqrt{A}$) for plinian tephra (Pyle, 1989). Fierstein and Nathenson (1992) used two proximal and distal exponential rates (κ) of the plot of log(T) against log ($\sqrt{A}$), which changed at the break in slope, in order to calculate the volume. Bonadonna and Houghton (2005) used a power method to estimate the volume of Plinian tephra deposits. When using the exponential method or the power formula, many isopachs are required to estimate the ashfall volume over large areas accurately.

* Nippon Koei Co., Ltd., 2, Kojimachi, 4-chome, Chiyoda-ku, Tokyo 102-0083, Japan.
** Public Works Research Institute, 1-6 Minamihara, Tsukuba-shi, Ibaraki 305-8516, Japan.
*** Deep Ocean Resources Development Company, Ltd., 1-3-15, Nihonbashi Horidome-cho, Chuo-ku, Tokyo 103-0012, Japan.
**** Ministry of Land, Infrastructure, Transport and Tourism, Osumi Office of River and National Highway, 1013-1 Shintomi, Kimotsuki-cho, Kimotsuki-gun, Kagoshima 893-1207, Japan.
† Sabo and Landslide Technical Center
†† Ministry of Land, Infrastructure, Transport and Tourism, Miyazaki Office of River and National Highway

Corresponding author: Yasuhisa Tajima
e-mail: tajima-ys@n-koei.jp

Fig. 1. Location of the Sakurajima volcano. Triangles denote active volcanoes.

Aramaki and Hayakawa (1982) developed a simple formula for the plot of log (T) against log(A), with a scaling exponent (power) fixed at -1. Hayakawa (1985) estimated the ejecta volume as $V=12.2\ T\times A$ (V: volume of tephra, A: area, T: thickness of tephra) with a constant of 12.2. This value of 12.2 was in agreement with results obtained from the crystal concentration method (Walker, 1980; 1981), in which the ejecta volume was estimated by the amount of plinian tephra observed on the ground. However, Pyle (1999) showed that the value of 12.2 was variable rather than constant.

We consider the geometrical concept of ashfall distribution, which does not require the collection or estimation of ashfall distribution or volume over large areas. For example, small island volcanoes require a volume estimate only for the limited area around the volcano. Recently, some authors considered that ashfall distribution would approximate the elliptical forms (Froggatt, 1982; Pyle, 1989; Sulpizio, 2005). Sulpizio (2005) calculated the approximate volume of tephra using elliptical distributions. In this study, we have developed an ellipse-approximated isopach (EAI) method based on a simple equation. We have applied this method to the volume

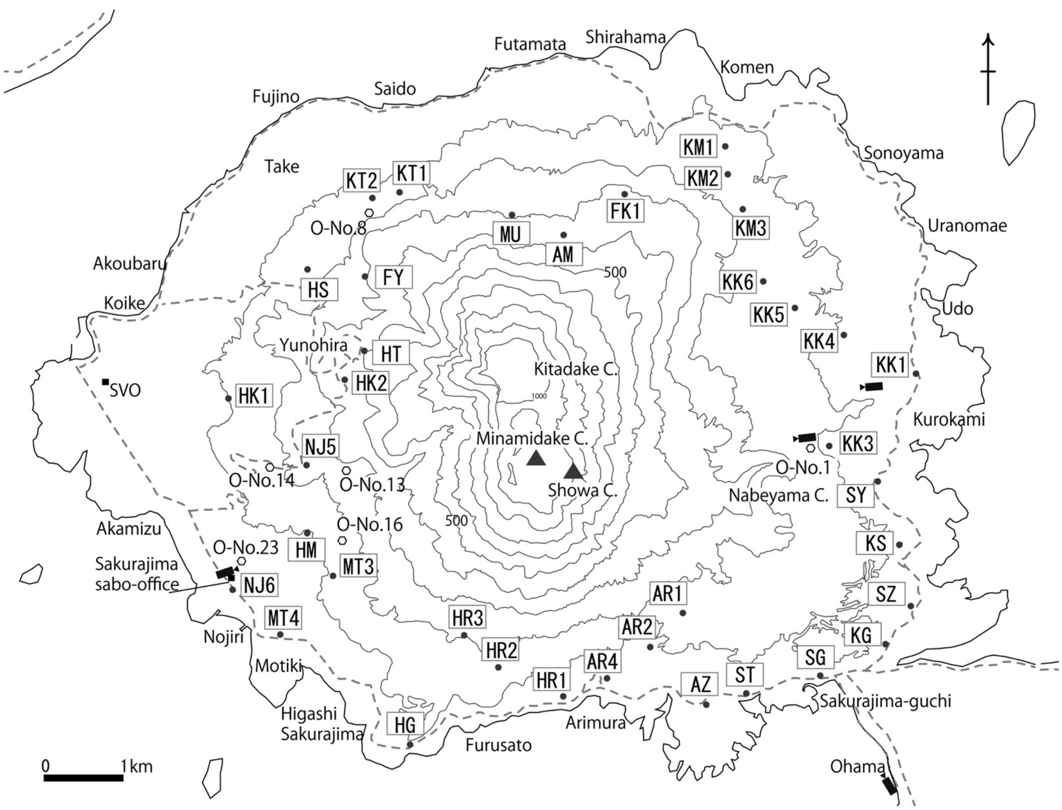

Fig. 2. Observation locations in Sakurajima. Solid circles denote locations of ash samplers for this study. Open circles denote monthly observation points and camera marks used by the Osumi Office of River and National Highway.

estimation of ashfall for ongoing eruptions of Skurajima volcano (Figs. 1 and 2), which have produced frequent thermal columns from vulcanian or ash eruptions. The depositional ashfall (tephra) volume and the ejecta ashfall (tephra) volume of an eruption are different meaning (Koyaguchi, 1996). In this study, we use the word "ashfall" to mean "depositional ashfall".

2. Ellipse-approximated isopach (EAI) method

2-1 Area-versus-thickness relationship

We use the relationship of the simple power function between log(T) and log(A) (see Eq. 1), where A is the area of one isopach, T is the thickness for that isopach, α is a coefficient and d is the exponent concerning T and A shown in equation (1). In this study, area (A) is given in square meters and thickness (T) in millimeters or grams per square meter.

$$A = \alpha T^{d} \tag{1}$$

It is uncertain whether the concept ($d = -1$) proposed by Aramaki and Hayakawa (1982) is appropriate for small phreatic, vulcanian or ashfall eruptions. We therefore review the relationship between ashfall thickness and area from recent vulcanian and phreatic eruptions in Japan. We use the described isopach maps to plot depositional area (m^2) versus thickness (m). In this case, we convert g/m^2 to m, using a depositional density of $1.5\,g/cm^3$ for the data produced by Yoshimoto *et al*. (2005) and Takarada *et al*. (2001).

At Shinmoedake volcano in the Kirishima volcanoes, southern Japan, phreatic eruptions started at 14 : 50 JST on February 17th, 1959, and continued for several days. An isopach map was drawn from 50 to 0 cm (Fig. 3; Fukuoka Meteorological Observatory, Kagoshima Local Meteorological Observatory and Miyazaki Local Meteorological Observatory, 1959). At Ontake volcano, central Japan, phreatic eruptions started from approximately 05 : 20 JST October 28th, 1979, until the following morning. The isopach map was based on observations around the volcano from October 30th to November 2nd, 1979 (Fig. 3; Yamada and Kobayashi, 1988). At Usu volcano, northern Japan, a phreatic eruption began on March 31st, 2000, from 13 : 07 JST until around 16 : 00. The small eruptions continued until September 2001 (Yamasato *et al*., 2002). Isopach maps were obtained for March 31st, April 1st and 2nd, and April 4th, 2000 (Fig. 3; Takarada *et al*., 2001). At Asama volcano, central Japan, an ash eruption started at 20 : 20 JST on September 1st, 2004 and some small eruptions continued until December 9th, 2004 (Nakada *et al*., 2005). Isopach maps were obtained for eruptions occurring on September 1st 20 : 02 JST, September 15th to 18th, September 23rd 19 : 44 JST, September 25th 18 : 36 JST, September 29th 12 : 17 JST, October 10th 23 : 10 JST, and November 14th 20 : 59 JST (Fig. 3; Yoshimoto *et al*., 2005). At Shinmoedake volcano, phreatic eruptions started

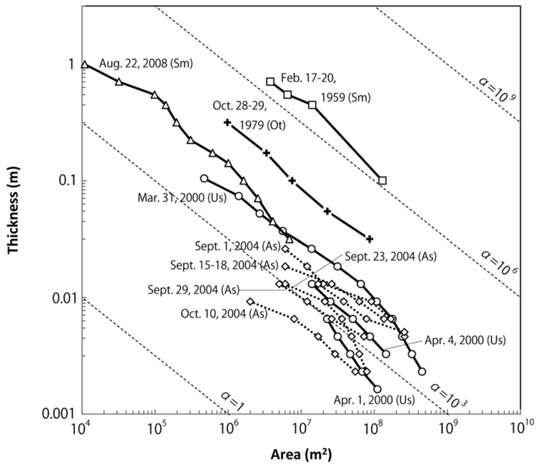

Fig. 3. Relationship between area (m^2) and thickness (m) of isopachs in several examples. Dashed lines denote vulcanian or small magmatic eruptions. Solid lines denote phreatic eruptions. Sm: Shinmoedake volcano in Kirishima, Ot: Ontake volcano, Us: Usu volcano, As: Asama volcano. Explanations of those isopachs are shown in section 2-1.

on August 22nd, 2008 and tremors continued for six hours, from 16 : 34 JST (the Japan Meteorological Agency website). An isopach map was presented for this eruption (Fig. 3; Geshi *et al.,* 2010). These results show that the area-versus-thickness relationship is $A = \alpha T^{-1}$, and that the phreatic and magmatic ashfall eruptions show a rate of same decrease ($d = -1$) in Fig. 3. In addition, the 1959-Shinmoedake, 1979-Ontake and 2008-Shinmoedake eruptions were comprised of multiple eruptions or a continuous eruption; those cases also showed a rate of decrease ($d = -1$). Therefore, we adopt a simple formula with the scaling exponent (power) fixed at approximately -1, as described by Aramaki and Hayakawa (1982). Regarding shapes of isopach, we assume that the tephra distribution approximates an ellipse that has the same aspect ratio (half radius of orthogonal axis/half radius of calculation axis) in concurrent eruptions (Fig. 4) with the correlation of A and T, following Eq. 1.

2-2 Formulation of EAI and the volume

The followings are three calculation ways of the ellipse-approximated isopach (EAI).

1) If the elliptical isopachs exhibit a fixed aspect ratio, we can calculate the ellipse-approximated isopach using one data point of the thickness or weight of the deposit and the determined calculation axis (one data point calculation).

2) If we do not know the aspect ratio of the elliptical isopach, we can calculate the ellipse-approximated isopach using two data points of the thickness or weight, and the

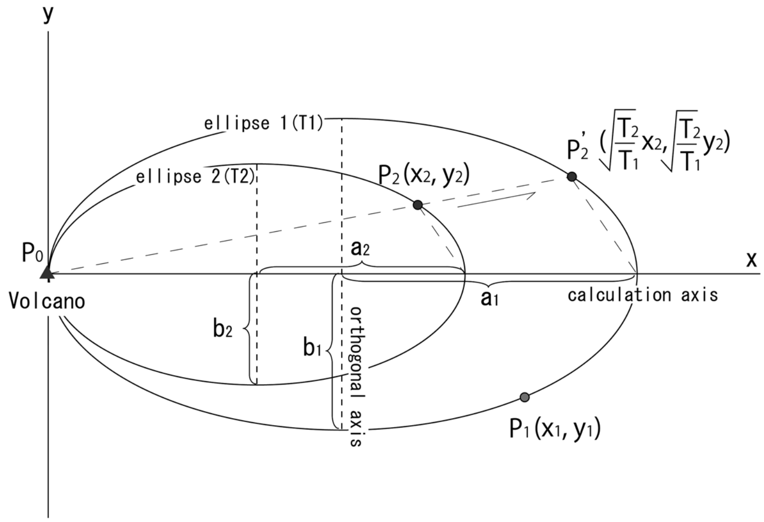

Fig. 4. Schematic representation of isopach drawn by ellipse approximation. The figure shows the EAI method for two data points. The x-axis represents the fixed dispersion (calculation) axis.

determined calculation axis (two data points calculation).

3) If the ellipse isopach does not exhibit an aspect ratio or an ellipse axis, we can calculate the ellipse-approximated isopach using three or more data points of the thickness or weight (multiple data points calculation).

Solution using one data point:

The elliptical isopach exhibits a fixed aspect ratio, defined as

$$\frac{b}{a}=c \tag{2}$$

where a is the calculation (ashfall distribution) axis of the ellipse; b, the orthogonal axis; and c, the aspect ratio.

A point (x, y) on the ellipse is given by

$$\frac{(x-a)^2}{a^2}+\frac{(y)^2}{b^2}=1 \tag{3}$$

The ellipse axes are determined from Eqs. 2 and 3 are

$$a=\frac{c^2x^2+y^2}{2c^2x},\ b=a\times c \tag{4}$$

Solution using two data points:

If ellipses 1 and 2 have the similar ellipse shapes (Fig. 4), then

$$\frac{b_1}{a_1}=\frac{b_2}{a_2} \tag{5}$$

From Eq. 1, $AT=\alpha$, and $A_1=\pi a_1b_1$ and $A_2=\pi a_2 b_2$. The relationship between ellipses 1 and 2 is

$$T_1a_1b_1=T_2a_2b_2 \tag{6}$$

From Eqs. 5 and 6,

$$\frac{a_2}{a_1}=\sqrt{\frac{T_1}{T_2}} \tag{7}$$

P_0 is source of ash distribution. If P_2 on ellipse 2 moves to a point on ellipse 1 using similar triangles shown by dash lines in Fig. 4, then

$$P_1=(x_1,y_1),\ P_2'=\left(\sqrt{\frac{T_2}{T_1}}x_2,\sqrt{\frac{T_2}{T_1}}y_2\right),\ P_0=(0,\ 0) \tag{8}$$

P_1 and P_2' on ellipse 1 are given by:

$$\frac{(x_1-a_1)^2}{a_1^2}+\frac{y_1^2}{b_1^2}=1 \tag{9}$$

$$\frac{\left(\sqrt{\frac{T_2}{T_1}}x_2-a_1\right)^2}{a_1^2}+\frac{\left(\sqrt{\frac{T_2}{T_1}}y_2\right)^2}{b_1^2}=1 \tag{10}$$

The ellipse axes are determined from Eqs. 9 and 10 as follows:

$$a_1=\frac{x_1^2y_2^2-x_2^2y_1^2}{2\left(x_1y_2^2-\sqrt{\frac{T_1}{T_2}}x_2y_1^2\right)},\ b_1=\sqrt{\frac{a_1^2y_1^2}{2a_1x_1-x_1^2}} \tag{11}$$

Solution using three data points:

If we consider three or more data points, any of the three approaches may be used to derive the solution. The three formulae are determined about the calculation axis (a), orthogonal axis (b), and calculation axis at a specified angle (θ). Here we show only the basic formulae.

We consider ellipses 1, 2, and 3, which have similar shapes:

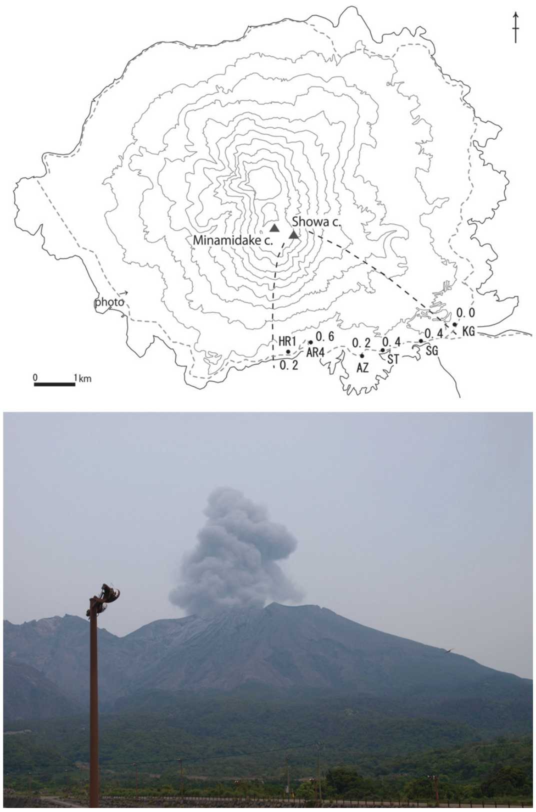

Fig. 5. The ashfall distribution and a photograph of the small eruption at 12 : 56 JST on April 28th. The values in the map are ash weights per square meter (g/m^2). The photograph was taken near NJ6 in Fig. 1.

$$\frac{b_1}{a_1}=\frac{b_2}{a_2}=\frac{b_3}{a_3} \tag{12}$$

Similarly to Eq. 6,

$$T_1a_1b_1=T_2a_2b_2=T_3a_3b_3. \tag{13}$$

The three points move according to a rotation matrix, for example:

$$\begin{pmatrix}x'_1\\y'_1\end{pmatrix}=\begin{pmatrix}x_1\cos\theta-y_1\sin\theta\\x_1\sin\theta+y_1\cos\theta\end{pmatrix}\begin{pmatrix}x'_2\\y'_2\end{pmatrix}=\begin{pmatrix}x_2\cos\theta-y_2\sin\theta\\x_2\sin\theta+y_2\cos\theta\end{pmatrix} \tag{14}$$

Eq. 14 is substituted into Eq. 11 and the two equations are solved numerically. Under natural conditions, it is impossible that three data points fit on an ellipse of one aspect at the same time.

The ashfall volume is calculated using the EAI as follows, using the distribution $A=\alpha\ T^{-1}$. The volume integral is:

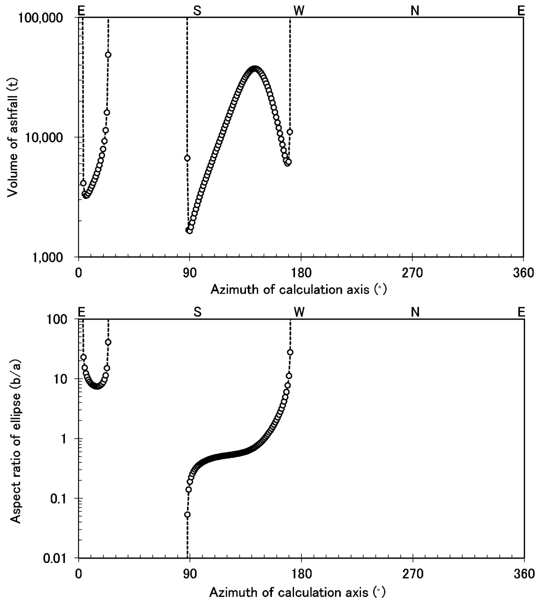

Fig. 6. The aspect ratio and volume of ashfall vs. calculation axis azimuth of the EAIs by the trial calculations of the two data points calculation. See the section 2-3 in the text for details of the calculation procedure.

$$V=\int_m^n AdT=(-\alpha\log(A_n))-(-\alpha\log(A_m)) \tag{15}$$

where m is the 10^4 m^2 area used by Takarada *et al*. (2001) and n is the area enclosed by the 0.1 g/m^2 isopach. The minimum observed thickness corresponded to a weight of 0.4 to 0.2 g/m^2 for the 12 : 56 JST eruption on April 28th at Sakurajima volcano (Fig. 5). Our field observations determined the lower threshold of detectable ashfall to be 0.1 g/m^2.

In this study, we discuss how to calculate for EAI (eq. 11) and estimate for the volume of tephra (eq. 15) using the two data points calculation.

2-3 Relationship between ellipse axis and volume of EAI

In this section, we demonstrate how to use the EAI method namely how to choose two data locations and set an ellipse axis. In the two data points calculation, it is very important to determine the calculation axis of the ellipse accurately. A trial calculation uses two data points for tentative ashfall amounts. The tentative amounts are set at sampling locations HR1 (100 g/m^2) and AR4 (50 g/m^2) at Sakurajima volcano (Fig. 7). Those are a value commonly observed at Sakurajima. The calculation results include ashfall volume and the aspect ratio of the ellipse, which is rotated from the calculation axis of the ellipse to one degree clockwise from due east (Fig. 6).

The axis of the ellipse is regarded as non-existent on the

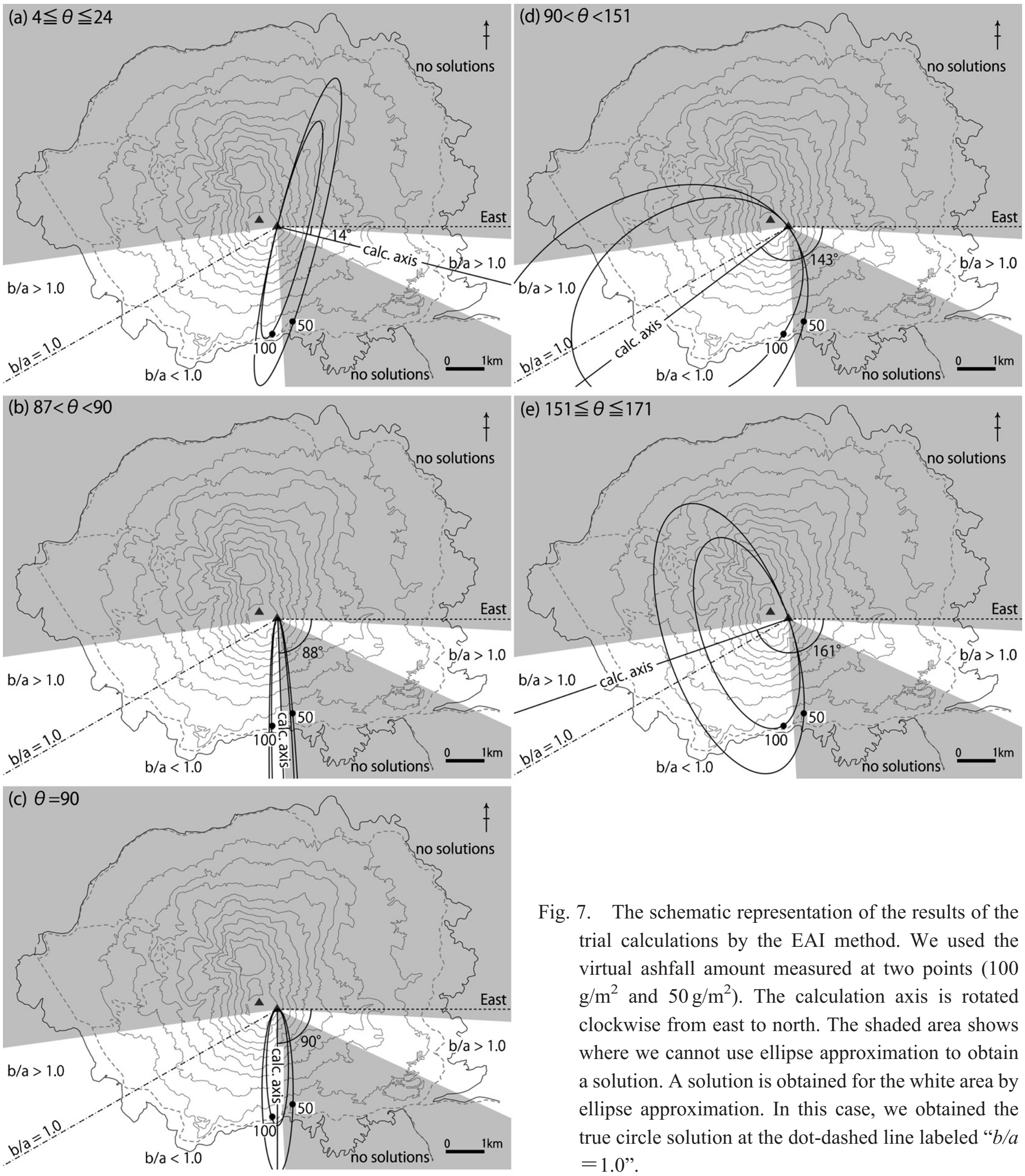

Fig. 7. The schematic representation of the results of the trial calculations by the EAI method. We used the virtual ashfall amount measured at two points (100 g/m^2 and 50 g/m^2). The calculation axis is rotated clockwise from east to north. The shaded area shows where we cannot use ellipse approximation to obtain a solution. A solution is obtained for the white area by ellipse approximation. In this case, we obtained the true circle solution at the dot-dashed line labeled "*b/a* = 1.0".

opposite side of the observation points ($171 < \theta < 4$). Firstly, the calculation axis of the ellipse is calculated to be four degrees clockwise from east. In this case, the aspect ratio is greater than one, meaning that the calculation axis is the short axis and the orthogonal axis is the long axis. The EAI distribution is a long orthogonal axis, which is an unusual result under natural conditions. The results are the same from 4° until 24° clockwise from due east (Fig. 7a). A solution can not be got past 25° ($24 < \theta \leq 87$), because the position of a low amount (50 g/m^2) interchanges a high amount (100 g/m^2) position for calculation axis in this area.

We must be careful in the case when the calculation axis is close to the observation point, which is a common case for the EAI calculation. The slight difference in the angle of the calculation axis leads to a larger change in the aspect ratio and the ashfall volume (Fig. 6). If the interval of the angle is very small, the infinite volume is taken between 87° and 88°, which results in an extremely elongated ellipse (Fig. 7b). It is considered that the narrow lateral distribution of ashfall is due to a very strong wind over a long period. The minimum ashfall volume occurred along 90°

(Figs. 6 and 7c) in this case. Next, the results are shown for an EAI example in which the ellipse calculation axis is located far from the observation points. The aspect ratio and the ashfall volume are much larger when the calculation axis is further from the observation points (Fig. 7d; $90<\theta<151$). The calculation axis is over 150° clockwise from due east, and the aspect ratio is reversed between the long orthogonal and short calculation axes of the ellipse (Fig. 7e; $151\leq\theta\leq171$), similar to Fig. 7a.

As described above, volume values from this calculation using ashfall information from only two points are variable depending on the axis. We will show how to determine the numerical value of the direction of calculation axis for the two data points calculation in Section 3, using the actual case of some eruptions at Sakurajima.

Ashfall sometimes distributes in concentric circles, as in the case of the 1991 Mt. Pinatubo eruption (Paladio-Melosantos *et al.*, 1996; Koyaguchi, 1996). In such cases, ashfall distributions cannot be constructed using the EAI calculation. Additionally, the EAI cannot provide results in cases where the distribution meanders.

2-4 Determination for ashfall amount at a particular point on EAI

The EAI method can calculate the weight or thickness at a particular point, from the established ellipse distribution. We calculate the half-radii of the short and long axes using Eq. 16, to determine the aspect ratio at any point of the ellipse. The calculation axis (a) is determined using Eq. 4, by substituting the known aspect ratio (c) at a particular point, where the thickness (T) is required. Additionally, the orthogonal axis (b) is determined using Eq. 4, and α is known. Therefore, Eq. 1 is substituted into Eq. 16, allowing us to find the weight or thickness (T) at a particular point as follows:

$$T=\alpha\times(\pi\times a\times b)^{-1} \tag{16}$$

2-5 Volume estimation by EAI for actual eruptions

The ashfall volumes of 2000 at Usu volcano (Takarada *et al.*, 2001; 2002) and those of 2004 at Asama volcano (Yoshimoto *et al.*, 2005) were calculated when the distribution axis was already known. Takarada *et al.* (2001) and Yoshimoto *et al.* (2005) estimated the segment isopachs volume using a log(T)-log(A) plot based on many observation locations. We estimated the volume using the data points by Takarada *et al.* (2001) and Yoshimoto *et al.* (2005). At first, we determined the direction of the major ellipse axis by straight isopach distributions near the vent, shown in the original studies. Next, we chose two data observation points for the calculation axis. The calculated volumes vary depending on the selection of two points. We compared the volumes obtained by actual observations (Takarada *et al.*, 2001 and Yoshimoto *et al.*, 2005) with the calculated EAI method results, which were nearest to those of actual observations (Fig. 8). The calculated values of EAI method are comparable to the actual observed values

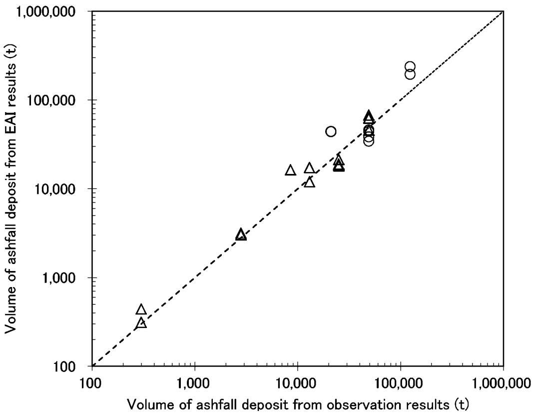

Fig. 8. Relation between the total volume of ashfall deposits and the volume calculated by the EAI method in the cases of the Usu 2000 eruptions and Asama 2004 eruptions (Table 1). The total volume of ashfall deposits are from Takarada *et al.*(2001) and Yoshimoto *et al.* (2005). Triangles denote the Asama eruptions in 2004, and circles denote the Usu eruptions in 2000.

(Table 1).

3. Application of EAI method to Sakurajima eruptions

In this section, we explain how to determine the ashfall volumes for the case at Sakurajima volcano.

3-1 Activity of Sakurajima volcano

Sakurajima is one of the most active volcanoes in Japan. Since 1955, small eruptions frequently have occurred at Minamidake crater (Kamo, 1974; Ishihara and Kobayashi, 1988; Ishihara, 1995). The pyroclasts, ballistics, and ashfalls have caused damage to houses and roads around the volcano. On June 4th, 2006, a vent in Sakurajima volcano, named Showa crater, opened on the east flank of Minamidake (Yokoo and Ishihara, 2007; Iguchi *et al.*, 2008). The crater then produced small eruptions in June 2006, and from May to June 2007.

Small pyroclastic density currents occurred at 10:18 and 15:54 JST on February 3rd, and 11:25 JST on February 6th, 2008 (JMA website). The surface activity was quiet until early April 2008. At 00:29 JST on April 8th, an eruption produced density currents and an eruption column more than 1 km above the vent. A small ashfall eruption with lithic fragments began on April 8th, and small eruptions continued, with short breaks, until mid-June. Small, short eruptions occurred after late June, and activity ceased in September. In most cases, the eruptions produced low columns, 500-3000 m in height. Showa and Minamidake craters have produced ashfalls even now.

3-2 Measurement of ashfall around the volcano

We applied our proposed method on the ashfall around Sakurajima volcano. Ash samplers, which consisted of

Table 1. The results of volume calclations by the EAI method using the data points of the Usu 2000 and Asama 2004 eruptions.

Volcano	Eruption day	Volume of ashfall (t)	Calculation case	Axis direction from east (°)	Calculation points 1 (g/m^2)	Calculation points 2 (g/m^2)	Volume of ashfall by EAI (t)	Precentage from original volume (%)
Usu	2001/03/31	124,000	case1	335.45	1154	1179	193,763	156
	*	*	case2		1179	107	237,188	191
	2001/04/04	49,000	case1	262.40	259	136	44,052	90
	*	*	case2		259	35	44,035	90
			case3		259	10	34,194	70
			case4		136	137	45,816	94
			case5		35	137	38,363	78
Asama	2004/09/01	49,000	case1	326.55	521	316	62,135	127
	**	**	case2		521	82	62,626	128
			case3		521	137	67,476	138
			case4		432	82	45,584	93
	2004/09/23	8,500	case1	289.95	268	59	16,291	192
	**	**	case2		268	29	16,307	192
	2004/09/25	300	case1	304.45	3.9	2.4	312	104
	**	**	case2		3.9	1.3	441	147
	2004/09/29	13,000	case1	264.10	403	221	17,311	133
	**	**	case2		403	31	11,977	92
	2004/10/10	2,800	case1	304.06	99	23	3,021	108
	**	**	case2		99	1	3,152	113
	2004/11/14	25,000	case1	352.80	891	454	18,910	76
	**	**	case2		891	337	21,322	85
			case3		891	204	18,559	74
			case5		891	137	18,071	72

* Takarada *et al.* (2001), ** Yoshimoto *et al.* (2005)

clear plastic cups of 7 to 8 cm diameter, were placed at three locations between February and April 2008. We tested the measurement error for this cup method at the southern and east part of the volcano set 13 samplers, and found that the observation errors were less than 4 %. After the increase in activity from April 2008, we placed additional ash samplers at 37 locations around the volcano on April 24th and 25th (Fig. 2). Ashfall deposits from the samplers were collected at different time intervals ranging from days to several weeks. The dates of retrieval were April 27th and 28th, May 1st, 7th, 9th, 18th, and 29th, June 5th and 14th, July 4th and 12th, August 1st and 30th, September 23rd, and October 18th. The ashfall characteristics were noted at the sampler locations in the field, after which the samplers were carefully covered with clear plastic cling-wrap and transferred to the laboratory. We soaked clumps of ash in distilled water to separate out smaller flakes. The deposit samples were dried and measured in terms of grams per square meter to determine the isopach. We converted g/m^2 to mm by applying the depositional density of the fresh ashfall deposit after the April 3rd–7th eruptions at sampling point AR1. We placed the ashfall deposits into a mould in order to undisturb the samples, which were

Table 2. Density of ashfall deposited by eruptions between Feb. 3rd and 7th, 2008.

Sample No.	Density of ashfall deposits under dry condition (g/cm^3)
AD-1	1.39
AD-2	1.63
AD-3	1.48
Average	1.50

then used to measure the depositional density under dry conditions. The resulting average depositional density is 1.5 g/cm^3 (Table 2), showing that an ashfall depth of 1 mm is equivalent to 1500 g/m^2.

3-3 The determination processes of ashfall axis

During observation periods, we determined the approximate directions of ashfall dispersion as follows (Table 3). Occasionally, observers remained at the volcano and noted the direction of the column. When we could not identify the distribution axis, we used web-cameras and other information. Our first source of eruption information was the website of the Japan Meteorological Agency[1] (JMA), which immediately releases eruption information, categorized by eruption time, column height, column direction, intensity, and other parameters. Next, we used images from web-cameras set up at the Osumi Office for River and National Highway of the Ministry of Land, Infrastructure, Transport and Tourism (MLIT)[2], and in the city of Tarumizu[3]. Kagoshima University (KU) also provided archives of their web-camera images[4], which yielded valuable information for determining the column direction (axis).

The determined ashfall directions described above usually have some uncertainties. Followings are the general procedure to determine the calculation axis exactly. If an eruption occurred once during an observation period, we chose generally the maximum observed amount (weight or thickness) at first near the expected distribution axis and next the second or third-largest value for the two data points of the EAI calculation. Next, we rotate an EAI calculation axis by step intervals of 1 to 2 degrees around the expected direction (we call this procedure as the step seeking hereafter) and calculate EAI distribution repeatedly every degrees. We can calculate the ashfall amounts of nearby locations, where the actual amounts of ashfall are measured using the EAI method and Eq. 16. Finally, we determined the EAI calculation axis so that the differences between the calculated and measured ashfall amounts become minimum value. The determination process is more easily when the exact direction is determined by the observation.

3-4 An example of general determination of EAI; June 28th, 2008 eruption

We explain how to determine the ashfall volumes for one eruption recorded at 06 : 36 JST on June 28th along with small eruptions on the afternoons of June 28th and 29th (JMA website). The ashfall of the small eruptions would be negligible in amount. We retrieved the samplers on July 5th. Ashfall was mainly found in the northern areas of the volcano. Ash weights of up to 263, 203 and 155 g/m^2 were recorded at sampling locations AM, FK1 and MU, respectively (Fig. 9). This ashfall originated from Showa crater after an eruption at 06 : 36 JST on June 28th. Based on the amount of ashfall, the distribution axis would pass through somewhere between locations AM and FK1. The angle of the EAI calculation axis was determined by the step seeking so that the calculation agreed with the weight recorded at other locations (KM2, KM1, KT1 and KT2) and limit of ashfall distribution (Table 3, calculation No. C58). The calculation axis was 275° clockwise from due east, and an EAI was drawn based on the data of locations AM and FK1 (Fig. 9). The location names and ashfall amounts of basic two data points and the appropriate ones are listed in Table 3. The estimated numerical values of the degree of axis are also listed.

3-5 An example in the case of the multiple eruptions; May 2nd to 7th, 2008 eruptions

When the interval of eruptions is shorter than that of retrieval of samples, it is very difficult to estimate the amount of each ashfall. We explain how to determine the ashfall volumes in the case of May 2nd to 7th observation period. During this period, four eruptions were recorded, at 06 : 34-06 : 50, 15 : 29, and 16 : 05-16 : 30 JST on May 6th and 06 : 38-06 : 54 JST on May 7th. Further smaller eruptions with negligible ashfall amounts also occurred on May 6th and May 7th (JMA website). During this period, the ashfall samples were retrieved once. Based on the amounts of the ashfall samples, mainly four distribution axes could be observed from the Showa crater towards locations HM, KG, ST and HR1 (Fig. 10). The observed ashfall informations suggested that these axes were corresponded to those of 06 : 34-06 : 50, 15 : 29, and 16 : 05-16 : 30 JST on May 6th; and 06 : 38-06 : 54 JST on May 7th eruptions, respectively (Fig. 10). The EAIs for these four eruptions were drawn, based on two data points calculation located near the corresponding axis with the step seeking using appropriate data points. Some locations used for the calculations were affected by ashfall of other eruptions, so that the affected weight must be taken away from the weights collected at locations (Table 3, calculation No.C13 to No.C18). We could use the estimation methods based on Eq. 16, as explained in 2-4.

3-6 The exceptional cases; April 11th, May 8th and June 1st

When eruptions continue steadily for a long time and the wind direction changes gradually, an obvious distribution axis cannot be determind for such eruptions. In this case, we estimate the ashfall volume by isopach area drawn by hand. We examine the relationship of $\alpha = TA$ (α : coefficient; T: m, A: m^2) from Eq. 1 to the volume of the deposits. For example eruptions continued for over 2 hours, from 14 : 13-16 : 45 JST, on May 8th (JMA website) and ash emission continued for some hours after 16 : 45 JST. The ashfall was mainly found in the northeast to north areas, and in the lower amounts in the northwest to west to south areas of the volcano. First, we determined four isopachs from the northeast to north by EAI (Table 3, calculation No.C19 to No.C22). In the western part, we produced the 30 g/m^2 isopach by hand. The ashfall volume of 11330 t on May 8th (Table 3) was estimated from the relation shown in Fig. 11. However, the main application for this relationship is limited only valid for volumes less than 100,000 tons.

---
[1] http : //www.seisvol.kishou.go.jp/tokyo/volcano.html
[2] http : //www.qsr.mlit.go.jp/osumi/camera_sabo.htm
[3] http : //camera19.city.tarumizu.kagoshima.jp/
[4] http : //volceye.edu.kagoshima-u.ac.jp/sakurajima.html

Table 3. List of Sakurajima eruptions from Feb. to Nov., 2008 and the results of the EAI volume calculation.

List of Eruptions by JMA						Volume calculation by EAI (1)									
								Point 1 for ellipse calculation				Point 2 for ellipse calculation			
Y/M/D	Time	Column height (m)	Direction	Class (Q)	Vent	Calcu -lation No.	Approximate axis direction	loc.	obs. (g/m^2)	subtracted value (s.v.) (g/m^2)	calc. (g/m^2)	loc.	obs. (g/m^2)	subtracted value (s.v.) (g/m^2)	calc. (g/m^2)
2008/2/3	0:39				Showa										
2008/2/3	10:18	> 1500	S-SE	3	Showa										
2008/2/3	15:54	> 1500		4	Showa										
2008/2/4	17:00				Showa	C01	Determined by geological observation near AR1.	AR1	3419.7		3419.7	O-No.20	810.0		810.0
2008/2/6	10:33	300		1	Showa										
2008/2/6	11:25	> 1000	SE	4	Showa										
2008/2/7	12:12	900			Showa										
2008/4/8	0:29	1200	SE	3	Showa	C02	Determined by JMA information.	AR1	285.6		285.6	AR2	470.3		470.3
2008/4/11	17:21	2200	SE	4	Showa	C03	Determined by JMA information.	AR4	123.1		123.1	–			
2008/4/11	21:09	2200	S	4	Showa	C04	Determined pass on AR1.	AR2	260.2	7.9(C03)	252.2	AR1	6.7	1.8(C03)	5.0
2008/4/12	11:15	1400	SW	3	Showa										
2008/4/13	5:59	> 1000	NE	3	Showa										
2008/4/13	7:03	> 1000	NE	3	Showa										
2008/4/14	2:31		uk	uk	Showa										
2008/4/14	14:16	1000	SE	3	Showa										
2008/4/15	13:55	1000	SE	3	Showa										
2008/4/15	14:49	1000	SE	3	Showa										
2008/4/21	16:19	1500	SW	3	Showa										
2008/4/27	12:08	1400	SE	3	Showa	C05	SG to AR4	SG	62.8	–	62.8	ST	37.0	–	37.0
						C06		AR4	40.2	1.3(C5)	39.0	AZ	29.3	9.6(C5)	19.7
2008/4/28	*12:56*		SE		Showa	C07	SG to AR4	SG	0.4	–	0.4	ST	0.4	–	0.4
						C08		AR4	0.6	–	0.6	HR1	0.2	–	0.2
2008/4/30	13:52	1500	W	3	Showa	C09	HK2	HK2	46.4	–	46.4	NJ5	20.6	–	20.6
2008/4/30	14:00				Showa	C10	AM	AM	26.4	–	26.4	MU	15.5	–	15.5
						C11		KS	1.9	0.6(C12)	1.3	SY	1.7	0.3(C12)	1.4
2008/5/1	6:52	300		1	Showa	C12	ST	ST	7.5	–	7.5	AR4	3.2	–	3.2
2008/5/6	6:34	1300	SW	3	Showa	C13	HM	HM	75.2	–	75.2	NJ5	2.6	–	2.6
						C14		HK2	3.7	–	3.7	HT	2.8	–	2.8
2008/5/6	15:29	1500	S	3	Showa	C15	KG to SG	KG	245.5	–	245.5	SZ	72.6	–	72.6
2008/5/6	16:05	1400	S	3	Showa	C16	ST to AZ	KK3	28.7	2.0(C15), 2.7(C17)	24.1	KK1	12.5	0.4(C15), 0.5(C17)	11.6
						C17		ST	253.6	17.3(C15)	236.3	AZ	217.8	5.3(C15)	212.4
2008/5/7	6:38	2400	S	3	Showa	C18	HR1	HR1	271.4	0.3(C17), 22.7(C16)	248.4	HR2	42.3	3.6(C16)	38.7
2008/5/8	14:13	2800	SE to N	4	Showa	C19	KK3 to FK1	SY	60.1	–	60.1	KK3	426.3	–	426.3
						C20		KK1	168.4	18.5(C19), 1.2(C21)	148.6	KK4	108.7	2.4(C19), 0.2(C20), 6.7(C21)	99.3
						C21		KK6	209.4	0.3(C19), 1.9(C22)	207.1	KM3	203.8	10.5(C22)	193.3
						C22		FK1	609.2	–	609.2	AM	39.3	–	39.3
2008/5/9	7:25	300–700		1											
2008/5/14					Showa	C23		SY	37.4	3.2(C26), 0.4(C25)	33.8	KK3	27.5	1.8(C26), 1.3(C25)	24.3
2008/5/15	4:51	1000	S	3	Showa	C24	HT	HT	479.1	–	479.1	HS	199.3	–	199.3
2008/5/15	20:03	1300	NE	3	Showa	C25	KM3 to KK6	KM2	107.6	–	107.6	KM3	358.4	–	358.4
2008/5/17	0:17	2000	SE	4	Showa	C26	AR4 to AZ	AZ	995.8	–	995.8	ST	510.2	–	510.2
2008/5/17	18:13	1500	S	3	Showa	C27	MT3 and HR3	MT3	208.5	–	208.5	MT4	73.9	–	73.9
						C28		HR3	90.2	7.5(C26), 0.3(C27)	82.4	HR2	45.7	20.7(C26)	25.0
2008/5/18	3:18	1600	N	3	Showa	C29	KT2 to AM	KT2	423.9	2.9(C24)	421.0	FY	283.7	49.3(C24)	234.4
						C30		MU	194.1	0.7(C25), 0.2(C24), 43.0(C29)	150.2	AM	101.8	3.1(C25), 13.1(C29)	85.6
2008/5/18	15:25	700	N	3	Showa	C31	KT1 to KT2	KT1	829.9	1.4(C37)	828.6	FY	124.8	13.7(C37)	111.1
2008/5/19	1:10	800	N	3	Showa	C32	AM to MU	AM	396.6	1.7(C36), 9.8(C31)	385.1	FK1	90.1	3.6(C36), 1.9(C31)	84.6
2008/5/19	19:56		uk	uk	Showa	C33	HR2	HR2	360.1	1.5(C34), 15.3(C35)	343.4	HR3	47.3	0.4(C34), 3.7(C35)	43.1
2008/5/20	0:22	2000	SW	4	Minamidake	C34	AZ to ST	AZ	1213.6	–	1213.6	SG	62.1	–	62.1
2008/5/20	21:00	2400	S	4	Showa	C35	HR1 to AR4	HR1	651.5	12.2(C35)	639.3	AR4	600.9	58.8(C35)	542.1
2008/5/21	16:21	1200	NE	3	Showa	C36	KK6 to KK5	KK6	161.5	–	161.5	KK5	223.6	–	223.6
2008/5/22	11:13	1300	NE	3	Showa	C37	HK2	HK2	353.2	–	353.2	HT	158.2	–	158.2
2008/5/23	23:57		uk	uk	Showa	C38	KM2	KM2	459.3	13.9(C36), 0.3(C31), 11.0(C32)	434.1	KM3	117.8	28.4(C36), 0.2(C31), 7.6(C32)	81.7
2008/5/30	14:20	1900	E	3	Showa	C39	MT4	MT4	291.7	–	291.7	NJ6	40.4	–	40.4
2008/5/30	14:52	1700	E	3	Showa										
2008/5/30	15:32	1800	Top	3	Showa										
2008/5/30	17:04	1200	W	3	Showa	C40	HR3	HR3	537.8	8.4(C39)	529.4	HR2	109.0	1.6(C39)	107.5
2008/5/30	18:44	1700	S	3	Showa										
2008/5/31	15:04	1900	S	3	Showa	C41	HR1 to AR4	HR1	236.0	4.9(C40)	231.1	AR4	184.5	1.8(C40)	182.7
2008/5/31	16:01	1500	S	3	Showa										
2008/5/31	16:41	1300	S	3	Showa	C42	AZ to ST	ST	164.5	0.5(C41)	164.0	AZ	138.1	0.2(C40), 2.0(C41)	136.0
2008/5/31	17:11	1300	S	3	Showa										
2008/5/31	17:58	1300	S	3	Showa	C43	SG	SG	97.5	2.9(C42)	94.5	KG	20.4	0.4(C42)	20.1
2008/6/1	1:41	2000	NE	4	Showa	C44	HK2 to HT	HK2	415.8	0.3(C39), 0.9(C44), 4.6(C45)	410.1	HT	419.8	2.7(C44), 29.6(C45)	387.5
2008/6/1	11:08	1200	NW	3	Showa	C45	KT2 to KT1	KT2	58.9	–	58.9	KT1	42.3	–	42.3
2008/6/1	11:42	1200	NW	3	Showa	C46	FY to HS	FY	202.7	17.6(C45)	185.2	HS	105.2	4.5(C45)	100.7
2008/6/1	12:49	1300	Top	3	Showa	C47	NJ5	NJ5	62.5	2.2(C39), 0.3(C44), 0.2(C45), 2.0(C46)	57.8	–		–	–
2008/6/9	2:34		uk	uk	Showa	C48	SG	SG	155.0	0.4(C53)	154.6	ST	25.7	–	25.7
2008/6/9	13:09	1000	S	3	Showa	C49	HR1 to AR4	HR1	39.1	0.2(C48), 2.2(C56)	36.7	AR4	28.3	0.8(C48), 0.9(C56)	26.5
2008/6/9	20:46		uk	uk	Showa	C50	KT1 to KT2	KT2	74.1	20.3(C57)	53.8	KT1	76.3	11.2(C57)	65.1
2008/6/10	10:23		uk	uk	Showa	C51	MU	MU	222.0	2.6(C50), 19.2(C57)	200.1	AM	133.1	1.1(C50), 6.2(C57)	125.9
2008/6/10	12:36		uk	uk	Showa										
2008/6/10	16:55		uk	uk	Showa	C52	KM1	KM1	146.0	0.2(C50), 0.2(C51), 2.8(C54)	142.8	KM2	26.2	0.2(C50), 0.2(C51), 4.4(C54)	21.5
2008/6/10	18:51		uk	uk	Showa										
2008/6/11	5:15		uk	uk	Showa	C53	KS	KS	23.4	–	23.4	SY	144.8	0.2(C54)	144.6
2008/6/12	0:09		uk	uk	Showa	C54	KK6	KK6	678.3	–	678.3	KK5	179.7	–	179.7
2008/6/12	2:37	2200	NE	4	Showa										
2008/6/12	10:39		uk	uk	Showa	C55	HK1	HK1	286.0	–	286.0	NJ5	11.2	–	11.2
2008/6/12	18:19	2200	SW	4	Showa	C56	HR3	HR3	172.1	–	172.1	HR2	25.7	–	25.7
2008/6/13	22:59	2400	NW	4	Showa	C57	HT to HK2	HT	824.6	7.3(C55)	817.4	HK2	579.4	92.5(C55)	486.9
2008/6/13	23:36	2500	NW	4	Showa										
2008/6/28	6:36		uk	uk	Showa	C58	AM to FK1	AM	262.9	–	262.9	FK1	202.7	–	202.7
2008/7/5	17:08	1600	E	3	Minamidake	C59	KK3	KK3	192.8	–	192.8	SY	29.4	–	29.4
2008/7/10	9:23				Showa	C60	MT4 to HM	MT4	65.3		65.3	HM	30.3		30.3
2008/7/14	5:08	1700	S	3	Showa	C61	HK2	HK2	173.1	–	173.1	HT	80.1	–	80.1
2008/7/14	6:19	1400	SW	3	Showa										
2008/7/25	11:18	1500	Top	3	Showa										
2008/7/25	15:56	1400	S	3	Showa	C62	KT2	KT2	48.5	1.8(C61)	46.7	KT1	33.3	1.1(C61)	32.2
2008/7/26	10:22	1500	NE	3	Showa										
2008/7/27	15:39	1300	NE	3	Showa										
2008/7/28	7:05	3300	N	4	Showa	C63	AM to MU	AM	1277.5	0.4(C62)	1277.2	MU	915.7	0.3(C61), 1.4(C62)	914.0
2008/7/28	10:10	3200	N	4	Showa										
2008/8/10	15:21	> 1800	NW	3	Showa	C64	FY to HS	FY	110.4	–	110.4	HT	48.8	–	48.8
2008/8/23	12:19		uk	uk	Minamidake	C65	AM to MU	AM	22.8	0.5(C64)	22.3	MU	23.0	1.2(C64)	21.8
2008/9/7	13:49	> 1200	Top	3	Showa	C66	HT to HK2	HT	21.0		21.0	HS	1.7		1.7
2008/10/3	17:35	1400	Top	3	Minamidake	C67	HR1 to HR2	HR1	3.9		3.9	HR2	0.6		0.6
						C68	ST	ST	1.5		1.5	AZ	0.6		0.6

The day and time and eruption center are from the JAM website. uk: unkown. Thick horizontal lines show collection times for ash fall samples. Multiple EAI distributions for one eruption were by continuously eruption with wind direction change or wind direction change depending on height. Locations (loc.) show in Fig. 2.

Table 3. continued.

Volume calculation by EAI (2)																	
Seeking point 1			Seeking point 2			Seeking point 3			Seeking point 4			Determin-ed Axis	Aspect Ratio	α	Volume		Comments on the seeking points and the volume estimation
loc.	obs. (g/m^2)	seeking (g/m^2)	loc.	obs. (g/m^2)	seeking (g/m^2)	loc.	obs. (g/m^2)	seeking (g/m^2)	loc.	obs. (g/m^2)	seeking (g/m^2)	(°)		(TS)	EAI (t)	Eruption (t)	
																7551	*In this period we observed two locations, so that the axis degree was determined exhaustively. Total EAI volume is 90,610 t (Feb. 3rd–7th). Main eruptions occurred on Feb. 3rd and 6th. The volume was divided in the ratio Q3 or uk/Q4 = 1:4
																7551	
																30203	
*												50	0.47	3878.1	90610	7551	
																30203	
																7551	
*												67	0.34	451.7	9100	9100	*In this time we observed at two locations, so that the axis degree was determined exhaustively.
*												111	—	1245.9	26990	27950	*In this period we observed at three locations for two distributions, so that the axis degree was determined exhaustively.
*												66	0.08	56.2	960		
																(5000)	Average volume of medium (Q3) classification.
																(5000)	
																(5000)	
																(5000)	
																(5000)	
																(5000)	
																(5000)	
																(5000)	
KG	8	11	SZ	8	3							43	0.20	127.4	2320	3690	
HR1	3	7	HR2	2	1	HR3	2	0	HG	0	0	71.5	0.22	78.5	1370		
KG	x	0										45	0.20	1.1	10	20	
AZ	0.2	0	HR2	x	0							81	0.27	0.6	10		
HT	15	18	FY	5	3	MT4	1	0	HG	x	0	195	0.28	94.0	1670	1670	
FK1	7	12	KM1	13	2	KT1	2	3	KT2	1	2	267.4	0.44	54.4	920	970	
KK3	1	1	KK1	2	0							8	0.28	4.0	50		
AZ	5	7	HR1	1	1	SG	2	4	KG	2	2	52.2	0.48	23.4	370	370	
MT3	1	7	MT4	1	1							167.15	0.12	57.2	970	1060	
FY	w	1										201.6	0.35	6.6	90		
KS	42	17	SG 1)	222	117	SY	5	4				31.5	0.18	516.9	10,510	10510	1) SG was affected by mainly C15 and C17. 2) AR4 was affected by mainly C17 and C18.
KK4	w	2										349.5	0.20	36.0	590	12920	
AR4 2)	102	75	SG 1)	222	102							53	0.39	599.5	12,330		
AR4 2)	102	29	HR3	10	5	HG	1	4				97	0.18	237.9	4,560	4560	
KS	4	3										354.2	0.12	277.7	5,390	49460	1) KK5 was affected by mainly C20 and C21. 2) KM1 was affected by mainly C21 and C22. Eruption continued for over 2 hours, from 14:13–16:45 JST. Ash emission some hours after 16:45 was calculated based on Fig. 11.
KK5 1)	35	6										339.6	0.08	485.9	9,840		
KM1 2)	81	34	KK5 1)	35	35							308.3	0.17	455.3	9,180		
KM1 2)	81	35										283	0.13	662.2	13,720		
															11,330		
KK1 1)	15	2	KS	w	9							2	0.21	55.8	950	950	
HK2	45	44										213.3	0.11	409.3	8,180	8180	1) KK1 was affected by mainly C23 and C25. 2) FK1 was affected by mainly C25 and C30. 3) HR1 was affected by mainly C26 and C28. 4) KT1 was affected by mainly C29 and C30.
KK6	358	306	KM1	41	64	KK1 1)	15	2	FK1 2)	55	9	308	0.17	803.9	16,890	16890	
AR4	638	610	HR1 3)	155	154	SG	179	106				64	0.33	2050.4	45,950	45950	
HM	5	5										155	0.08	143.7	2,650	3810	
HG	15	29	HR1 3)	155	2							124	0.25	67.0	1,160		
KT1 4)	392	341										233.6	0.23	953.4	20,270	27030	
KT1 4)	392	54	FK1 2)	55	18							252	0.36	342.5	6,760		
HS 1)	45	28	KT2	624	612							237	0.16	1262.6	27,380	27380	1) HS was affected by mainly C31 and C37. 2) KM1 was affected by mainly C32 and C38. 3) HR3 was affected by mainly C33 and C35.
MU	392	343	KM1 2)	69	11							261	0.33	743.8	15,540	15540	
HR3 3)	47	31										111	0.17	208.8	3,960	3960	
ST	1076	1121	KG	29	19	SZ	4	6				55	0.19	1695.5	37,510	37510	
AZ	c	8	HR3 3)	47	4							88	0.16	740.6	15,460	15460	
KK1	22	23										323	0.30	422.2	8,460	8460	
HS 1)	45	24										201.6	0.20	367.1	7,280	7280	
KM1 2)	69	54										299.2	0.03	565.5	11580	11580	
HR3	c	8	NJ5	c	2							151	0.15	406.8	8130	15020	Total eruption volume of C39 and C40 include on May 30th from 14:20 to 18:44 JST eruptions.
MT4	c	5	HR1	c	5							124	0.20	348.9	6890		
HR2	c	4	AZ	c	2							88	0.14	271.1	5250	11810	Total eruption volume of C41 to C43 include on May 31th from 15:04 to 17:58 JST eruptions.
AR4	c	2	SG	c	3							56	0.10	219.2	4180		
SZ	1	3										37	0.13	130.1	2380		
HK1	2	8										205.9	0.10	443.4	8920	8920	
MU	w	2										233.5	0.17	98.1	1750	1750	
KT2	c	9										221	0.12	187.3	3530	3530	
NJ6	c	2										182	–	73.0	1270	1270	
KG	24	28	SZ	5	5							39.5	0.17	216.1	4110	4110	
HR2	c	4										90	0.27	44.5	740	740	
FY	152	25										238	0.29	169.4	3160	3160	
KM1	c	0										261	0.10	305.3	5970	5970	Total eruption volume of C51 includes on June 10th at 10:23 and 12:36 JST eruptions.
KK6	c	0										295	0.03	46.5	780	4200	Total eruption volume of C52 and C53 include on June 10th and June 11th eruptions.
KK3	35	59										2	0.16	182.0	3420		
KM2	c	4										317	0.11	543.1	11090	2218 8872	The eruption volume is divided in the ratio uk/Q4 = 1:4 on June 12th.
HM	1	1										195	0.08	450.6	9070	9070	
MT4	13	18										133	0.24	250.5	4820	4820	
FY	152	134										209	0.23	931.4	19770	19770	
KM1	57	47	KM2	42	45	KT1	4	13	KT2	6	8	275	0.40	598.6	12310	12310	
KS	2	1	KK1	1	1							359	0.07	122.0	2220	2220	
NJ6	29	30	HG	5	7							150	0.33	207.5	3940	3940	
NJ5	17	19										200	0.24	220.6	4210	4210	Eruption volume of C61 includes on July 14th eruptions.
HS	w	3										233.5	0.16	73.7	1280	1280	Eruption Volume of C62 includes on July 25th, 26th and 27th eruptions.
KM1	7	2	KM2	w	2	KM3	w	1				262.2	0.12	1850.4	41180	41180	Eruption volume of C63 includes on July 28th eruptions.
HS	77	72	KT2	16	19	KT1	9	8	HK2	22	13	221	0.21	167.0	3110	3110	
FK1	6	11	KM1	2	1							270	0.29	38.5	630	630	
HS	2	3	HK1	1	1							207	0.18	21.8	340	340	
HR3	w	0	AR4	w	2							89	0.09	6.7	90	130	
SG	0	1	KG	0	0							45	0.21	3.0	40		

The "obs." values are observation weight. The subtracted values (s.v.) are calculated using Eq.16. The "calc." values are weight for two data points calculation (calc.＝obs.－s.v.). The "seeking" values are calculated weight on seeking point using Eq. 16. w, weak ashfall; x, no ashfall; c: other EAI calculation point.

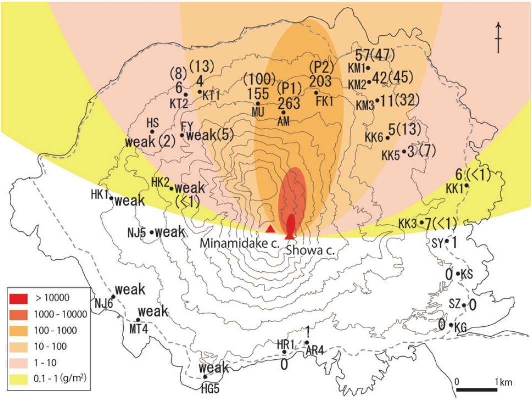

Fig. 9. Spatial distribution of the amounts of the ashfall based on the EAI calculation for 06 : 36 JST on June 28th at Sakurajima. The values are ash weights per square meter (g/m^2) and the values in parentheses are calculated weights. P1 and P2 weights show in Table 3 (Calculation No. C58).

In the cases of April 11th and June 1st, we calculated the ashfalll using only one observation location. In these cases, we estimated the ashfall volume by the one data point calculation with the averaged aspect ratio of EAI. The aspect ratio of 0.21 was taken from average value in Table 3. The ashfall volumes were calculated to be 26990 t for April 11th and 1270 t for June 1st were estimated (Table 3, calculation No.C03 and No.C47).

4. Discussion

4-1 Comparison ashfall volume between EAI estimations and monthly MLIT observations

The Osumi Office of the MLIT, using 0.57 m-diameter drum-type samplers, measured the weight of monthly ashfall in several observation locations (Fig. 2). To validate our method, we compare the observed monthly weights obtained by the Osumi Office with the accumulate weight derived using the EAI distributions. We use Eq. 16 to calculate the tephra thickness for eruptions at the six observation locations of the Osumi Office shown in Table

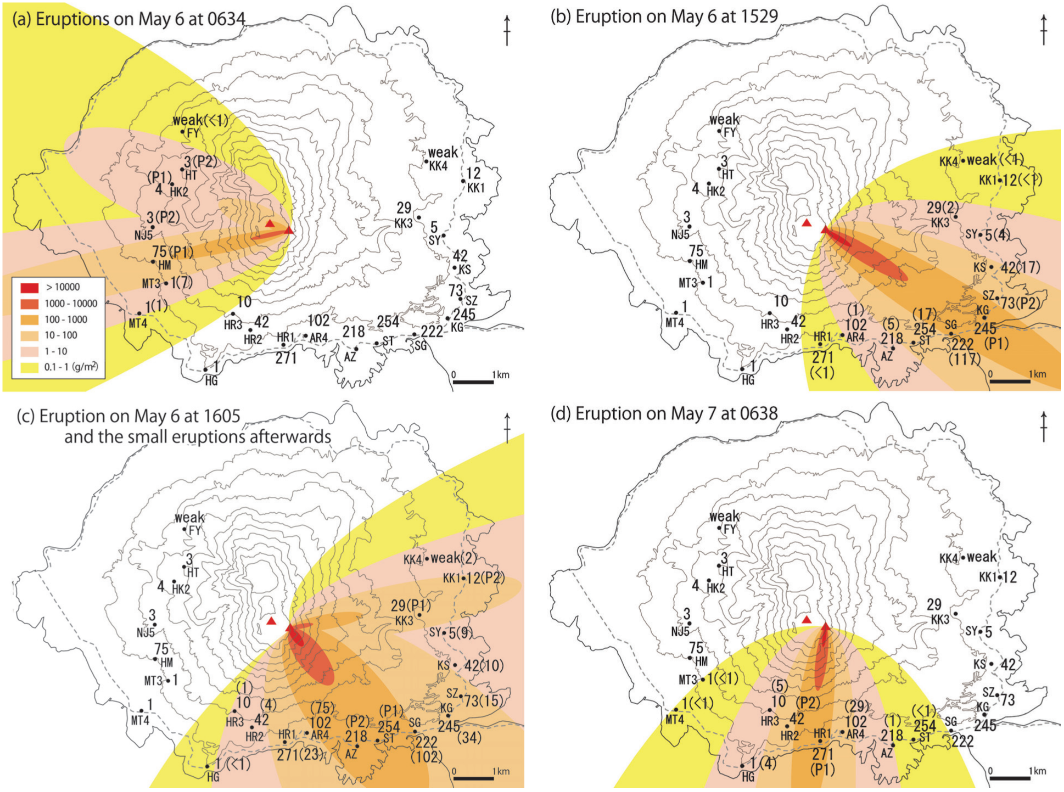

Fig. 10. Spatial distributions of the amounts of the ashfall based on the EAI calculation for May 2nd to 7th eruptions. In this period, four eruptions were recorded: from 06 : 34 to 06 : 50 JST on 6th (a: No.C13, C14), at 15 : 29 JST on 6th (b: No. C15), 16 : 05 JST on 6th (c: No.C16, C17), and 06 : 38 JST on 7th (d: No.C18). The values are ash weights per square meter (g/m^2) and the value in parentheses are calculation weights. P1 and P2 weights and calculation No. show in Table 3.

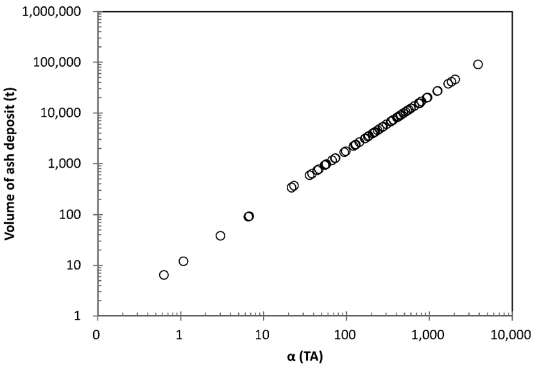

Fig. 11. The relationship between α and volume of ash deposit. The values of α and volume are shown in Table 3.

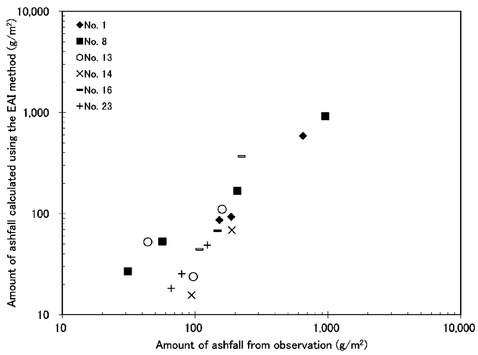

Fig. 12. The relationship between monthly amount (from May to August) of ashfall observed by the Osumi Office of MLIT and the monthly amount calculated using the EAI method. The Osumi Office observation locations are shown in Fig. 2 (*e.g.* O-No. 1). Plotted ashfall amounts are over 10 g/m^2.

4. The data from the six observed locations show a positive correlation with our calculations (Fig. 12, Table 4). The observed values tend to be higher than the calculated ones for some data points, due to the intervals between observation locations. We note that the slightly higher observation values would be caused sometimes by contamination of the secondary ash.

4-2 Temporal variation of ashfall volume estimated by EAI method during 2008 activity

Using combined eruption informations and our observations at Sakurajima, we were able to determine the 68 directions of EAI dispersion and estimated 58 (66) eruption volumes (Table 3).

1) Volume for JMA classifications

According to the JMA classification scheme, the scale of the eruptions covers seven categories (Q1-Q7). These categories are determined by the area size (m^2) of the eruption column by eye-watching observation. (Japan Meteorological Agency, 1994). Based on our EAI data, the average volume produced in the Q3 (medium) classification, which is most common at Sakurajima volcano, is about 5000 t, whereas the average volume produced in the Q4 (rather much) classification is about 20000 t in this study. Thus it is resonable to consider that the volume is divided according to the classification of JMA as Q3 : Q4 = 1 : 4 (Table 3).

2) Temporal change of ashfall volume during 2008 activity

During 2008, the first volcanic activity occurred from February 3rd to 7th. We estimated the ashfall volume of each eruption between February and October 2008, using the EAI method which the exhaustively axis determined by geological observation or JMA information (Table 3). The daily and cumulative volumes of ashfall are shown in Fig. 13. An eruption occurred from April 8th to April 21st, which continued until June 13th. During April 21st to June 3rd period the eruption rate increased. Ashfall amounts were not collected for the eight eruptions that took place on the 12th to the 25th of April. Instead we used the medium-classification average volume of 5000 t (Table 3) because the eruptions during this period were classified as “medium (Q3)” according to JMA. The peak volumes of the eruptions were clustered from May 6th to 23rd, 2008 (Fig. 13). The rate of eruption decreased in the next period from June 14th to July 28th. The pace of activity subsequently changed during August, with a single eruption every two or three weeks from the Showa crater; after October, there were a number of very small eruptions from the Minamidake crater. Using this method, we are able to reveal temporal change of the ashfall volumes, which is very important information in predicting the progress of the ongoing eruption.

Table 4. Ashfall volume of EAI estimations and monthly Osumi Office observations.

Location	May		June		July		August	
	Observed (g/m^2)	Calculated (g/m^2)	Observed (g/m^2)	Calculated (g/m^2)	Observed (g/m^2)	Calculated (g/m^2)	Observed (g/m^2)	Calculated (g/m^2)
O-No.1	648	584	187	93	152	86	17	0
O-No.8	952	914	208	167	57	53	31	27
O-No.14	0	34	189	68	94	16	48	1
O-No.16	224	367	148	68	108	44	22	0
O-No.23	124	49	79	25	66	18	31	0

5. Conclusion

The EAI provided a swift geometric method for assessing ashfall eruptions. In many cases, the distributions calculated using the EAI method correlated well with the observed data for the Usu and Asama volcanoes, in which small eruptions recently produced low columns. Under

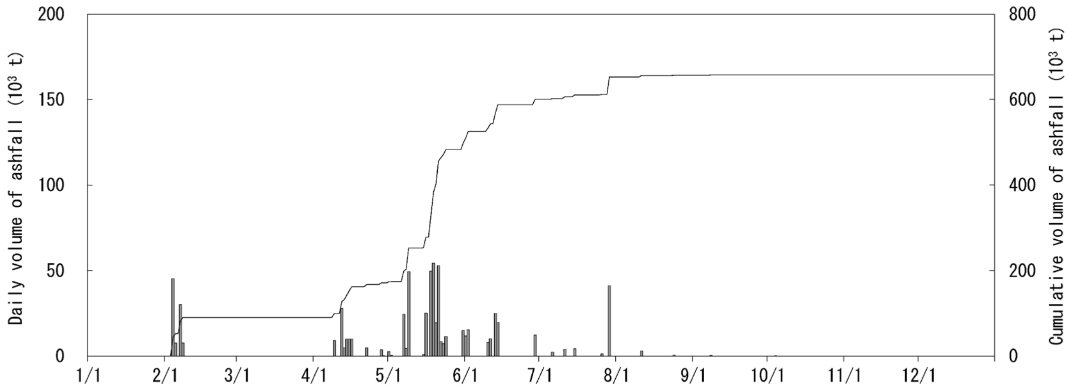

Fig. 13. Temporal changes of ashfall volumes determined by the EAI method. The column bars denote the daily ashfall volumes determined by the EAI method, and the step line represents the cumulative volume.

these conditions, we could approximate the ashfall distribution as a single exponential function. The EAI method is useful for small, continuous eruptions and for small island volcanoes where terrestrial ashfall is naturally limited to the area of the island. When using the EAI method, it is important to determine the correct EAI calculation axis and to confirm the fit between several observation points and the calculated distribution.

Acknowledgments

We sincerely thank Mr. S. Shimomura and Mrs. K. Kikuchi of the Research and Development Center Laboratory of Nippon Koei, and Mr. N. Takezawa of PWPI and Mr. A. Kubota of Kagoshima University in the field. We are grateful to the JMA for information, the prefecture of Kagoshima, the city of Tarumizu, and the Education Department of Kagoshima University. We also thank Drs. T. Kobayashi and N. Kinoshita of Kagoshima University, Dr. M. Iguchi of Kyoto University, and Dr. H. Itoh of Iwate Prefectural University for their helpful comments. We also thank Dr. M. Ban editor and reviewers of this manuscript who made devoted efforts in a long reviewing process. We thank Mr. D. Uehara of Monashu University for the helpful English comments. Finally, we deeply thank Mrs. M. Tajima for her useful suggestions.

References

Aramaki, S. and Hayakawa, Y. (1982) Ash fall during the April 26, 1982 eruption of Asama volcano. *Bull. Volcanol. Soc. Japan*, **27**, 203–215 (in Japanese with English abstract).

Bonadonna, C. and Houghton, B. F. (2005) Total grain-size distribution and volume of ash fall deposits. *Bull. Volcanol.*, **67**, 441–456.

Fierstein, J. and Nathenson, M. (1992) Another look at the calculation of fallout tephra volumes. *Bull. Volcanol.*, **54**, 156–167.

Froggatt, P. C. (1982) Review of methods of estimating rhyolitic tephra volumes; application to the Taupo Volcanic Zone, New Zealand. *J. Volcanolo. Geotherm. Res.*, **14**, 301–318.

Fukuoka Meteorological Observatory, Kagoshima Local Meteorological Observatory and Miyazaki Local Meteorological Observatory (1959) Eruption of Shinmoedake, Kirishima volcano, on 17 February, 1959 (Showa 34 Nen 2 Gatsu 17 Nichi no Kirishimayama Shinmoedake no Bakuhatsu). 16p (in Japanese).

Geshi, N., Takarada, S., Tsustui, M., Mori, T. and Kobayashi, T. (2010) Products of the August eruption of Shinmoedake volcano, Kirishima volcanic group, Japan. *Bull. Volcanol. Soc. Japan*, **55**, 53–64 (in Japanese with English abstract).

Hayakawa, Y. (1985) Pyroclastic geology of Towada volcano. *Bull. Earthq. Res. Inst., Univ. Tokyo*, **60**, 507–592.

Iguchi, M., Tameguri, T. and Yokoo, A. (2008) Volcanic activity during the period from 1997 to 2007. In *10th Joint Observation of Geophysics and Geochemistry* (Iguchi, M. ed), 1–18. Ann. Dist. Prev. Res. Inst., Kyoto Univ. Japan (in Japanese).

Ishihara, K. and Kobayashi, T. (1988) Recent volcanic activity at Sakurajima volcano (Commentary on Photogravures). *Bull. Volcanol. Soc. Japan*, **33**, 269–271 (in Japanese).

Ishihara, K. (1995) Sakurajima. In *National Project for Prediction of Volcanic Eruptions*, 161–168. Japan Meteorological Agency (in Japanese).

Ishimine, Y. (2007) Overview of diverse computer simulations and their potential contribution to volcanology. *Bull. Volcanol. Soc. Japan*, **52**, 221–239 (in Japanese, with English abstract).

Japan Meteorology Agency (1994) Manuals for volcanic observations (Kazan Kansoku Shishin; volume of observation). Japan Meteorology Agency, 318p (in Japanese).

Japan Meteorology Agency Website. http://www.seisvol.kishou.go.jp/tokyo/volcano.html (7/22/2012).

Kagoshima University Website. http://volceye.edu.kagoshima-u.ac.jp/sakurajima.html (7/22/2012).

Kamo, K. (1974) Recent volcanic activity of Sakurajima volcano. *Bull. Volcanol. Soc. Japan*, **19**, 48 (in Japanese).

Koyaguchi, T. (1996) Volume estimation of tephra-fall deposits from the June 15, 1991, eruption of Mount Pinatubo by theoretical and geological methods. In *Fire and mud, eruptions and lahars of Mount Pinatubo, Philippines* (Newhall, C. G., and Punongbayan, R. S., eds), 583–600. Philippine Institute of Volcanology and Seismology and University of Washington.

Nakada, S., Yoshimoto, M., Koyama, E., Tsuji, H. and Urabe, T. (2005) Comparative study of the 2004 eruption with old eruption at Asama volcano and the activity evaluation. *Bull. Volcanol. Soc. Japan*, **50**, 303–313 (in Japanese with English abstract).

Osumi Office of River and National Highway, of the Ministry of Land, Infrastructure, Transport and Tourism. Website: http://www.qsr.mlit.go.jp/osumi/camera_sabo.htm (7/22/2012).

Paladio-Melosantos, M. L., Solidum, R. U., Scott, W. E., Quiambao, R. B., Umbal, J. V., Rodolfo, K. S., Tubianosa, B. S., Delos Reyes, P. J., Alonso, R. A. and Ruelo, H. R. (1996) Tephra falls of the 1991 eruptions of Mount Pinatubo. In *Fire and mud, eruptions and lahars of Mount Pinatubo, Philippines* (Newhall, C. G., and Punongbayan, R. S., eds), 513–535. Philippine Institute of Volcanology and Seismology and University of Washington.

Porter, S. C. (1973) Stratigraphy and chronology of late Quaternary tephra along the South Rift Zone of Mauna Kea volcano, Hawaii. *Geol Soc. Amer. Bull*., **84**, 1923–1940.

Pyle, D. M. (1989) The thickness, volume and grain size of tephra fall deposits. *Bull. Volcanol*., **51**, 1–15.

Pyle, D. M. (1999) Widely dispersed Quaternary tephra in Africa. *Global and Planetary Change*, **21**, 95–112.

Rose, W. I., Bonis, S., Stoiber, R. E., Keller, M. and Bickford, T. (1973) Studies of volcanic ash from two recent Central American eruptions. *Bull. Volcanol*., **37**, 338–364.

Sulpizio, R. (2005) Three empirical methods for the calculation of distal volume of tephra-fall deposit. *J. Volcanolo. Geotherm. Res*., **145**, 315–336.

Suzuki, T. (1981) "Thickness-Isopach area" curve of tephra. *Bull. Volcanol. Soc. Japan*, **26**, 9–23 (in Japanese with English abstract).

Takarada, S. *et al*., (2001) Volcanic ashfalls from the Usu 2000 eruption and situation at the source area. *Bull. Geol. Surv. Japan*, **52**, 167–179 (in Japanese, with English abstract).

Takarada, S., Hoshizumi, H., Miyagi, I., Nishimura, Y., Miyabuchi, I., Miura, D. and Kawanabe, Y. (2002) Proximal deposits of the Usu 2000 eruption. *Bull. Geol. Surv. Japan*, **47**, 645–661 (in Japanese, with English abstract).

Tarumizu city website: http://camera19.city.tarumizu.kagoshima.jp/ (1/9/2009).

Thorarinsson, S. (1954) The eruption of Hekla 1947–48, part 2, Ch. 3, The tephra-fall from Hekla on March 29, 1947. *Soc. Sci. Islandia*. Reykjavik, 1–68.

Walker, G. P. L. (1980) The Taupo pumice: product of the most powerful known (ultraplinian) eruption? *J. Volcanol. Geotherm. Res*., **8**, 69–94.

Walker, G.P.L. (1981) Plinian eruptions and their products. *Bull Volcanol*., **44**, 223–240.

Yamada, N. and Kobayashi, T. (1988) Geology of the Ontakesan district. With Geological Sheet Map at 1 : 50,000, Geol. Surv. Japan, 136p. (in Japanese, with English abstract).

Yamasato, H., Miyamura, J., Mori, H., Usui, Y., Sakuma, K., Watanabe, A., Sato, J., Takahashi, Y. and Sakai, T. (2002) Eruptive activity inferred from infrasound associated with the 2000 eruption of Usu volcano. *Bull. Volcanol. Soc. Japan*, **47**, 255–262 (in Japanese, with English abstract).

Yokoo, A. and Ishihara, K. (2007) Volcanic activity around Showa crater of Sakurajima volcano monitored with infrared and video cameras. *Annals of Disas. Prev. Res. Inst., Kyoto Univ.*, **50**, 149–155.

Yoshimoto, M. *et al.* (2005) Mass estimation and characteristics of ejecta from the 2004 eruption of Asama volcano. *Bull. Volcanol. Soc. Japan*, **50**, 519–533 (in Japanese, with English abstract).

(Editorial handling Masao Ban)

桜島火山における楕円近似による火山灰堆積量の推定法について

田島靖久・田村圭司・山越隆雄・津根　明・鶴本慎治郎

海に囲まれた火山島では観測できる場所が限られ，火山灰の堆積量を推定することが困難であった．また，火山灰が大量に降ることによって交通，健康，農作物へ影響を生じ，厚く堆積した斜面では土石流が発生しやすくなる．ゆえに火山灰の降下量（降灰量）や分布を迅速に把握する方法の開発は，火山学，防災学上の重要な研究対象となる．このため桜島のように海に囲まれ観測場所が限られる火山での迅速かつより少ない点から火山灰の堆積分布・量を推定する方法を検討した．我々は等層厚線が相似の楕円に近似されると仮定し，各点から得られる楕円近似した等層厚線の軸比を一定とし，分布を幾何学的に単純化した．また，降灰観測データの豊富な噴火事例を検証した結果，面積=層厚が $A=\alpha T^{d}$（T: 層厚，A: 面積）とした場合，その減衰はほぼ−1 乗に近似可能である．これらの関係より，火口位置などを楕円の軸端点とし，火山灰堆積分布に相当する分布軸が決められる場合，計算上 2 点の観測値から火山灰堆積量を推定することが可能となる．ただし，本手法では通常，計算軸を求める際に，計算に使用する 2 点以外の 1〜4 点程度の複数観測点の値が必要となる．本手法については分布軸が精度良く求められることと，複数の観測値を解析結果が矛盾なく説明できることを適応条件とした．本手法を用い桜島 2008 年の活動について 60 を超える噴火の火山灰堆積量を推定した．推定した分布から特定の場所における月ごとの累積降灰量を計算した結果は観測量を再現可能である．2008 年の桜島の活動を日単位の堆積量として解析すると，ピークは 5 月 6〜23 日頃であったと推定される．本方法を適応することによって，これまで観測が難しかった火山島での火山灰堆積量観測が可能となる．